Dynamic Uni- and Multicellular Patterns Encode Biphasic Activity in Pancreatic Islets

Manon Jaffredo, Eléonore Bertin, Antoine Pirog, Emilie Puginier, Julien Gaitan, Sandra Oucherif, Fanny Lebreton, Domenico Bosco, Bogdan Catargi, Daniel Cattaert, et al.

Dynamic Uni- and Multicellular Patterns Encode Biphasic Activity in Pancreatic Islets

Manon Jaffredo,[1] Eléonore Bertin,[1] Antoine Pirog,[2] Emilie Puginier,[1] Julien Gaitan,[1] Sandra Oucherif,[1] Fanny Lebreton,[3] Domenico Bosco,[3] Bogdan Catargi,[1,4] Daniel Cattaert,[5] Sylvie Renaud,[2] Jochen Lang,[1] and Matthieu Raoux[1]

Diabetes 2021;70:1–11 | https://doi.org/10.2337/db20-0214

Biphasic secretion is an autonomous feature of many endocrine micro-organs to fulfill physiological demands. The biphasic activity of islet β-cells maintains glucose homeostasis and is altered in type 2 diabetes. Nevertheless, underlying cellular or multicellular functional organizations are only partially understood. High-resolution noninvasive multielectrode array recordings permit simultaneous analysis of recruitment, of single-cell, and of coupling activity within entire islets in long-time experiments. Using this approach, we addressed the organizational modes of both first and second phase in mouse and human islets under physiological and pathophysiological conditions. Our data provide a new uni- and multicellular model of islet β-cell activation: during the first phase, small but highly active β-cell clusters are dominant, whereas during the second phase, electrical coupling generates large functional clusters via multicellular slow potentials to favor an economic sustained activity. Postprandial levels of glucagon-like peptide 1 favor coupling only in the second phase, whereas aging and glucotoxicity alter coupled activity in both phases. In summary, biphasic activity is encoded upstream of vesicle pools at the micro-organ level by multicellular electrical signals and their dynamic synchronization between β-cells. The profound alteration of the electrical organization of islets in pathophysiological conditions may contribute to functional deficits in type 2 diabetes.

Biphasic secretion is a common physiological feature in a number of hormone and neuro-hormone–secreting micro-organs (1–4). Pancreatic islets represent a well-described model of biphasic secretion (4,5): a first peak phase (5–15 min) is followed by a decrease in the secretion rate, called nadir, and a subsequent second long-lasting plateau phase (6,7) and installation of pulsatility (8). Insulin secreted during the first phase immediately reaches the liver to rapidly regulate blood glucose levels. The second phase targets more distant organs as long as glycemia remains elevated (9). This optimized kinetic is strongly altered during aging and in type 2 diabetes (10–14). As biphasic insulin profiles persist ex vivo (6), multiorgan feedback loops are not required, and patterns are encoded at the micro-organ level.

Although the phenomenon per se has been extensively described, it is still not understood how this phasic organization is achieved and what drives the progression from first to second phase. β-Cell metabolism has been monitored via mitochondrial membrane potential, oxygen consumption, or metabolic coupling factors. Metabolism increases upon glucose stimulation, with, often (15,16), but not always (17,18), a discrete and brief peak of 1–2 min during the first phase before raising again during the nadir while secretion decreases; thus, these metabolic profiles do not explain secretion patterns. The organization of insulin-secreting vesicles in distinct functional pools in β-cells has been widely invoked to explain biphasic secretion (19–21). Interestingly, biphasic activation is a multicellular process since it is profoundly altered in dissociated islets and connexin-36 knockout mice (22,23). Hence, vesicle pool

[1]University of Bordeaux, CNRS, Institute of Chemistry and Biology of Membranes and Nano-objects, UMR 5248, Pessac, France
[2]University of Bordeaux, CNRS, Institut Polytechnique de Bordeaux, Institute of System Integration, UMR 5218, Talence, France
[3]Department of Surgery, Cell Isolation and Transplantation Center, Geneva University Hospitals, University of Geneva, Geneva, Switzerland
[4]University of Bordeaux, Hôpital Saint-André, Endocrinology and Metabolic Diseases, Bordeaux, France
[5]University of Bordeaux, CNRS, Institute of Cognitive and Integrative Neurosciences, UMR 5287, Bordeaux, France

Corresponding author: Matthieu Raoux, matthieu.raoux@u-bordeaux.fr

Received 2 March 2020 and accepted 11 January 2021

This article contains supplementary material online at https://doi.org/10.2337/figshare.13562354.

organization may not represent the main determinator of biphasic activation in islets.

Different approaches have been used to investigate multicellular processes in islets. Analysis of intraislet connectivity by dynamic imaging has provided an elegant model of highly active leader cells (24,25), in line with β-cell heterogeneity (26), but requires complex mathematical offline reconstruction and potential bias (24,27). In addition, the existence of such hub cells is still debated (28), and inherent restrictions have limited such experiments to short periods. Consequently, they do not inform about the dynamic evolution throughout different phases and about the behavior of the entire micro-organ.

We have therefore sought for a more direct approach endowed with high temporal resolution (kHz) and useable throughout the hours of postprandial islet activation, a situation in which rundown in optical and classical electrophysiological approaches may occur. Analysis of extracellular electrical field potentials with multielectrode arrays (MEAs) of intact islets avoids such drawbacks (29,30). Both unicellular and multicellular signals can be observed in the form of single-cell action potentials (APs) (29,31) and multicellular slow potentials (SPs) for hours or even days (30,32). SPs represent robust and specific signals propagated among β-cells via connexin-36 in both rodent and human islets (32). Hence, this approach provides a dynamic, direct, and unbiased measurement of unicellular and of micro-organ behavior via APs and SPs.

We have therefore addressed the question how biphasic activity of pancreatic islet micro-organs is encoded in terms of single-cell and coupled electrical activity throughout a physiological time span and how this is disrupted in pathophysiological states.

RESEARCH DESIGN AND METHODS

Mouse Islets

Adult male C57BL/6J mice (10–20 weeks of age, except for Fig. 7*A* and *B*: 12–45 weeks) were sacrificed by cervical dislocation according to University of Bordeaux ethics committee guidelines. Islets were obtained by enzymatic digestion and handpicking (29,30,32). MEAs were coated with Matrigel (2% v/v) (BD Biosciences, San Diego, CA), and intact islets were seeded (one pancreas per MEA) and cultured at 37°C (5% CO_2, >90% relative humidity) in RPMI medium (11 mmol/L glucose, except for glucotoxic conditions: 20 mmol/L in Fig. 7*C* and *D*) (Thermo Fisher Scientific, Waltham, MA) as described (29,30,32).

Human Islets

Human islets (healthy donors; for details, see Supplementary Materials) were isolated at the Geneva Cell Isolation and Transplantation Center (29,32), distributed through the European Consortium for Islet Transplantation, and authorized by the ethical committee (Comités de Protection des Personnes; 16-RNI-10). Human islets were cultured on MEAs under the same conditions as mouse islets but using CMRL-1066 medium (5.6 mmol/L glucose, except for glucotoxic conditions) (Thermo Fisher Scientific) (29,32).

MEAs

Different MEAs (Multi Channel Systems GmbH [MCS], Reuttlingen, Germany) were used to address specific questions. Standard MEAs (60MEA200/30iR-Ti-gr, 59 titanium nitride electrodes [TiN], Ø 30 μm, 200 μm interelectrode distance) permitted the recording of SPs of ~1 islet/electrode (1.0 ± 0.1 islets/electrode, $n = 49$ islets, $N = 3$ independent preparations). Recordings of different intraislet regions were performed using high-density MEAs (HD-MEAs) (60HexaMEA40/10iR-ITO-gr, 59 TiN electrodes, Ø 10 μm, 40 μm interelectrode). Both MEAs were continuously perifused at 0.5 mL/min (Reglo ICC; Ismatec, Glattbrugg, Switzerland).

To measure simultaneously electrical parameters and insulin secretion (ELISA 80-INSMSU-E01; ALPCO, Salem, NH), microfluidic MEAs (μMEAs) were developed using MEA200/30iR-Ti-gr with a microfluidic channel (Ø 0.8 mm) in polydimethylsiloxane and perfused at 8 μL/min (MFCS-EZ; Fluigent, Villejuif, France). Kinetics of medium changes were determined as published (30).

Finally, poly(3,4-ethylenedioxythiophene) (PEDOT) and carbon nanotube–covered MEAs (PEDOT-MEAs) (60Pedot-MEA200/30iR-Au-gr, electrode arrangement as in standard MEAs) were used to detect APs, which are hardly discernable otherwise (29), and solutions were replaced by pipetting to avoid mechanical artifacts.

Extracellular Electrophysiological Recordings

MEA recordings were performed at 37°C, pH 7.4 (29,32), in solutions containing 1.2 mmol/L $CaCl_2$ for mouse islets (2.5 mmol/L in Supplementary Fig. 5*B–D*) or 1.8 mmol/L for human islets as published previously (29,32), which is close to physiological levels and provides sufficient driving force for SP quantification. When specified, a solution without $CaCl_2$ was applied to evaluate basal activity. Glucagon-like peptide 1 (GLP-1) solutions (Bachem Bio-Science Inc, King of Prussia, PA) were prepared ex tempore. Electrodes with noise levels >30 μV peak-to-peak were regarded as artifacts, connected to the ground, and not analyzed (3.6 ± 1.7% of electrodes; $N = 5$). Extracellular field potentials were acquired at 10 kHz, amplified, and band-pass filtered at 0.1–3,000 Hz with a USB-MEA60-Inv-System-E amplifier (MCS; gain: 1,200) or an MEA1060-Inv-BC-Standard amplifier (MCS; gain: 1,100), both controlled by MC_Rack software (v4.6.2, MCS).

Intracellular Recordings

Intracellular recordings were performed simultaneously with extracellular recordings on standard MEAs. Intracellular potentials of islet cells were measured by current-clamp (10 kHz sampling rate, 10 kHz low-pass filter) with sharp glass Clark micropipette microelectrodes (Harvard

Apparatus, Les Ulis, France) filled with 3 mmol/L KCl (96 ± 18 mol/LΩ; $n = 17$) and coupled to an Axoclamp-2B amplifier (Molecular Devices, San Jose, CA) controlled by Spike2 software (v7.01; Cambridge Electronic Design Ltd, Cambridge, U.K.). A common reference electrode was used for both recordings. An electrical artifact observable on both recordings was used to synchronize intra- and extracellular traces.

Quantifications

Images of islets on MEAs were taken before and after each experiment to localize electrodes covered with islets (44.1 ± 7.4% of electrodes; $N = 5$ independent preparations). Islet cell monolayer surfaces were quantified with ImageJ software (v1.52d; National Institutes of Health, Bethesda, MD). Electrophysiological data were analyzed with MC_Rack software. SPs and APs were isolated using a 2-Hz low-pass filter or a 3–700-Hz band-pass filter, respectively, and frequencies were determined using the threshold module of MC_Rack with a dead time (minimal period between two events) of 300 ms (SPs) and 10 ms (APs). The peak-to-peak amplitude module of MC_Rack was used to determine SP amplitudes. Simultaneous extra- and intracellular recordings were analyzed with Spike2 software.

Analysis of Intraislet Synchrony

After filtering at 2 Hz, SPs were detected using the peak detection module of Spike2 with a threshold of −15 μV. The degree of synchrony between SPs on electrodes was computed with MATLAB (vR2012B; MathWorks, Natick, MA) following a method based on Schreiber et al. (33), originally used to compute synchronization between trains of neuronal spikes (Supplementary Methods and Supplementary Fig. 1).

Data Presentation and Statistical Analysis

Experiments were replicated on at least three independent biological preparations, except when indicated. If not stated otherwise, N represents the number of independent preparations and n the number of electrodes analyzed. Graphics, quantifications, and statistics were performed with Prism software (v7; GraphPad, La Jolla, CA). Data are presented as means and SEM or whiskers boxes (box, 25th to 75th percentiles; line in the middle of the box, median; + or ■, mean; and whiskers, 10–90th percentiles). The minimal value of mean SP frequency after the first peak (corresponding to the nadir) was taken as the limit between phases.

Gaussian distributions were tested by D'Agostino-Pearson test and comparison of two groups with paired data by two-tailed paired t tests or nonparametric t tests with Wilcoxon matched-pairs signed-rank test. Two groups with unpaired data were compared using two-tailed unpaired t tests or nonparametric Mann-Whitney tests. For more than two groups, one-way ANOVA with Tukey post hoc or nonparametric Dunn tests were used.

Data and Resource Availability

Data sets generated and/or analyzed during the current study are available from the corresponding author upon reasonable request.

RESULTS

Biphasic Glucose-Induced Insulin Secretion Is Encoded by Multicellular SPs

Intact mouse islets were cultured on MEAs (Fig. 1*A*) to record noninvasively extracellular field potentials. As previously described, two types of signals were observed (Fig. 1*B*): the well-known unicellular APs and the more recently described SPs (29,30), which are of multicellular origin and require β-cell coupling via connexin-36 (32). We first monitored the frequency and amplitude of SPs in islets to determine whether they correlate to well-known biphasic secretion patterns. When islets were stimulated by an increase in glucose from 3 mmol/L to the moderate concentration of 8.2 mmol/L (Fig. 1*C*), a clear biphasic electrical profile of SPs was triggered, in terms of both frequencies and amplitudes (Fig. 1*C*). Each phase owned a specific electrical "signature": SPs of high frequencies but small amplitudes in the first phase and lower frequencies but increasing amplitudes during the second phase (Fig. 1*D*). Hence, electrical coupling modes of islet β-cells are biphasic and develop in a dynamic fashion.

Another known insulin secretagogue, L-leucine, bypasses glycolysis. Stimulating the same islets with either glucose or leucine (Fig. 1*E*), the first electrical phase was comparable between the two molecules in terms of peak of SP frequencies. However, in the case of leucine, SPs were largely reduced in the second phase (Fig. 1*E* and *F*). Thus, the metabolism of the main stimulator (i.e., glucose) triggers a full second electrical phase, while leucine may require coactivation of additional metabolic pathways, such as by glutamine (34).

By introducing μMEAs (Fig. 2*A* and *B*), we simultaneously recorded SPs and insulin secretion (Fig. 2*C*). Biphasic kinetics of SP frequencies were highly correlated with biphasic insulin secretion (Fig. 2*C*). Moreover, maximal correlation was obtained when both SP frequencies and amplitudes were taken into account (Fig. 2*C* and *D*), supporting the view that multicellular SPs, upstream of secretory pools, constitute the main regulator of biphasic insulin secretion.

Intraislet Electrical Coupling Enlarges Considerably in the Second Phase

The magnitude of extracellular electrical signals often mirrors the degree of cell synchrony, at least in the brain (35). We hypothesized that the increase of SP amplitude during the second phase was due to an increase in β-cell synchrony within an islet. Since standard MEAs do not offer spatial resolution below the dimensions of a single islet (Supplementary Fig. 2*A*), we used HD-MEAs providing ∼10 times more electrodes per islet, which permitted multisite analysis of single islets without affecting the

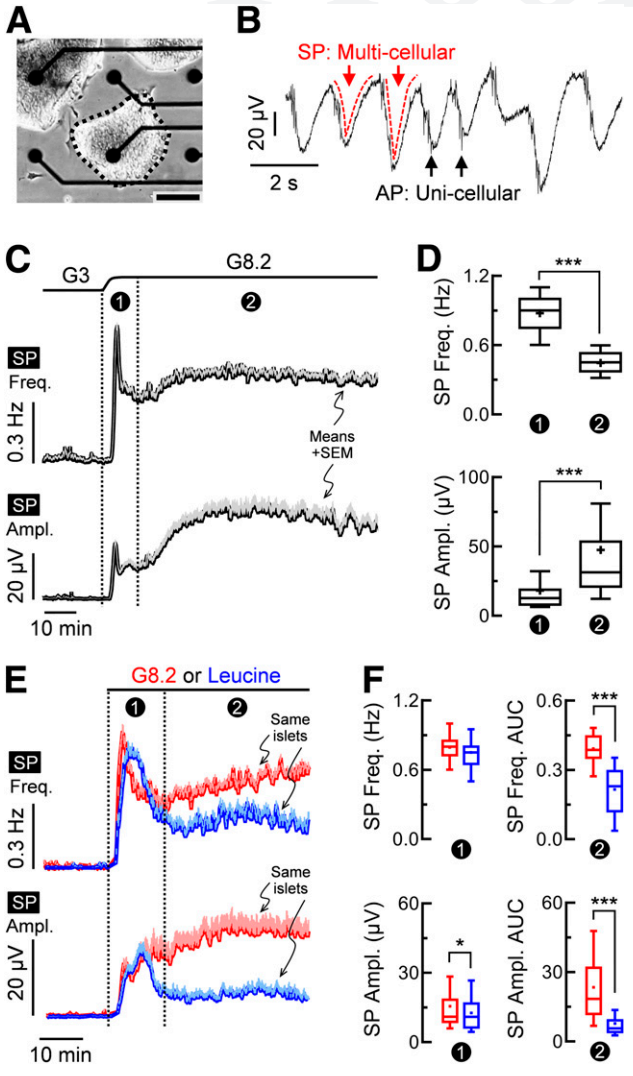

Figure 1—A physiological increase in glucose induces a biphasic electrical profile of SPs. *A*: Mouse islet (dotted line) on an extracellular electrode of a MEA. Scale bar: 100 µm. *B*: Recording from one MEA-electrode when islets are maintained at 8.2 mmol/L glucose shows two types of electrical signals: multicellular SPs and unicellular APs. *C*: Mouse islets were stimulated by an increase in glucose from 3 to 8.2 mmol/L. As in all figures, ❶ and ❷ indicate the first and the second phase, respectively, and glucose concentrations are indicated as G followed by the concentration in millimoles per liter (e.g., G8.2 for 8.2 mmol/L glucose in this figure). Mean + SEM of SP frequencies (Freq.) and amplitudes (Ampl.) were reported ($N = 7$, $n = 104$). See RESEARCH DESIGN AND METHODS for the optical determination of the kinetics of changes in glucose concentrations (black line at the top). *D*: Statistics on data in *C*. Top panel: peak frequency of SPs during the first phase and mean frequency during the second phase (>25 min after glucose change) were determined for each electrode. Bottom panel: mean amplitude during the two phases. *E*: Islets were first stimulated with glucose (red, 3–8.2 mmol/L). At >100 min later, the same islets were stimulated with L-leucine (blue, 20 mmol/L in the presence of G3) and kinetics of SP frequencies and amplitudes were compared. Note that, under these conditions, two consecutive electrical responses to G8.2 were similar ($N = 5$). *F*: Statistics on data in *E* ($N = 2$, $n = 29$). Left: peak frequencies and mean amplitudes during the first phase. Right: AUCs of SP frequencies and amplitudes during the second phase normalized over time. *$2P < 0.05$; ***$2P < 0.001$.

signal-to-noise ratio (Supplementary Fig. 2*B*). The two electrical phases of SPs were again clearly observable regarding frequencies and amplitudes (Supplementary Fig. 2*C* and *D*) and pulsatility appeared after 40–60 min with a mean pulse period of ~4 min (Supplementary Fig. 2*D*–*F*), similar to insulin secretion data (8,36). Note that islet inactivation following glucose decrease was rapid (<5 min) and not phasic (Supplementary Fig. 2*C* and *D*). In the representative HD-MEA illustrated in Fig. 3, two electrodes covered by the same islet were compared with each other (intraislet) and to a third electrode contacting another islet (interislets) (Fig. 3*A*). All three electrodes revealed SPs of high frequencies and small amplitudes during the first phase and the inverse during the second phase (Fig. 3*B*). The increase in SP amplitudes in the second phase was concomitant with a clear synchronization of SPs within a given islet, but not between different islets (Fig. 3*B*). Such absence of interislet synchrony suggests that extraislet mechanisms are involved in the whole pancreas synchrony during pulsatile secretion (8,36). A dynamic MATLAB code was then developed to quantify the degree of interelectrode synchrony during the biphasic activation (Supplementary Methods and Supplementary Fig. 1). At 3 mmol/L glucose, islets rarely generated SPs, and consequently, intraislet synchronies were absent (Fig. 3*C*, left). When islets were stimulated by 8.2 mmol/L glucose, the different regions within the same islet partially synchronized in the first phase (Fig. 3*C*, middle), and this intraislet synchrony considerably increased during the second phase (Fig. 3*C*, right). Statistical comparisons confirmed specific electrical coupling modes for each phase, and SP synchrony was positively correlated with amplitude and negatively correlated with frequency (Fig. 3*D*). SP amplitude represents a direct, nonbiased, and continuous measurement of intraislet connectivity, and thus, synchrony is accompanied by the generation of larger functional clusters of lesser activity.

We further addressed the nature of the SPs and islet β-cell coupling by simultaneous extracellular and intracellular recordings. To that end, standard MEAs were used: SPs were measured on a microelectrode at steady state during the second phase, while membrane potentials were recorded with sharp microelectrodes introduced into cells located at different positions within the same islet (Fig. 3*E*). Single-cell recordings showed slow and regular plateau depolarizations (Fig. 3*E*), also known as slow Ca^{2+} waves (18,37). Up to four cells within the same islet were investigated: regardless of their position, intracellular plateau depolarizations were always synchronized with SPs captured via the MEA-electrode located at the bottom of the islet (Fig. 3*E*). Glucose responses were observed in the majority of cells (63.6%), and 85.7% of them were synchronized with extracellular SPs (Fig. 3*F*). Hence, multicellular SPs represent summations of synchronized intracellular slow plateau depolarizations of β-cells. These data also indicate that electrical coupling concerns almost the entire islet during the second phase.

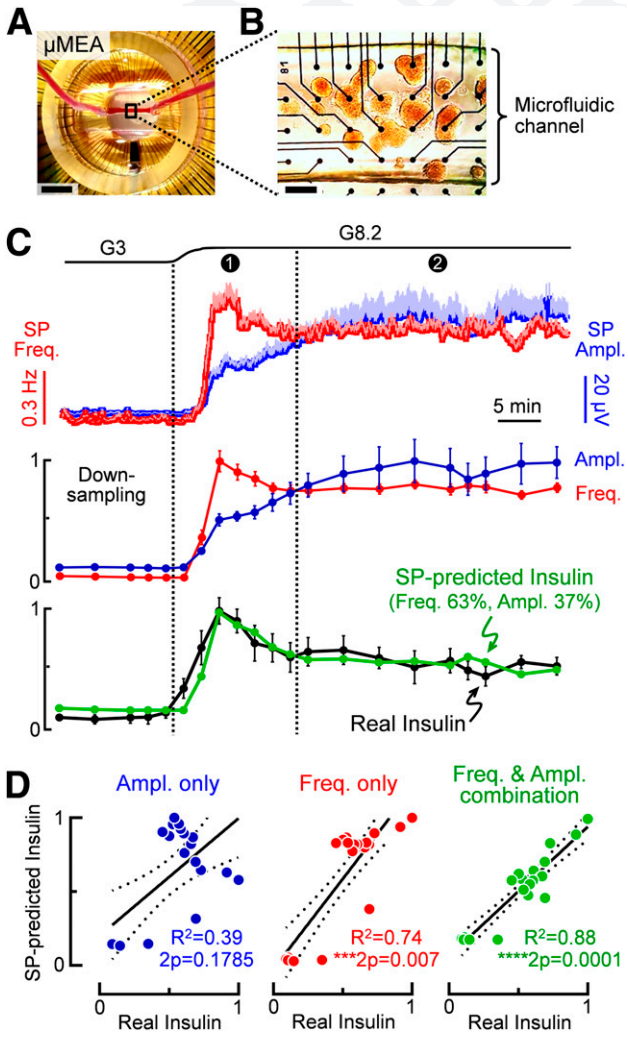

Figure 2—Combination of SP frequencies and amplitudes is highly correlated with biphasic insulin secretion, as shown with μMEAs. *A*: Image of a μMEA loaded with a phenol red solution showing the microfluidic channel at the center. Scale bar: 0.5 cm. *B*: Mouse islets cultured in the microfluidic chamber. Scale bar: 200 μm. *C*: Simultaneous measurements of SP frequency (Freq.), SP amplitude (Ampl.), and insulin secretion in μMEAs provide correlations between SP and insulin biphasic kinetics. *C*, top: islets were stimulated by an increase in glucose from G3 to G8.2, and kinetics of SP Freq. and Ampl. (means + SEM) were monitored during the first (❶) and second (❷) phase (n = 18 islets from N = 4 independent experiments). *C*, middle: SP Freq. and Ampl. (means ± SEM) were normalized and resampled to match insulin sampling periods. *C*, bottom: "Real Insulin" in black is the normalized insulin secretion (means ± SEM; N = 4 independent experiments). In green, "SP-predicted Insulin" represents the optimal combination of SP Freq. and Ampl. with the formula: SP-predicted Insulin = a × Freq. + b × Ampl. + c, where a = 1.15 ± 0.14, b = −0.67 ± 0.14, and c = 0.23 ± 0.05 (SD; R^2 = 0.88). *D*: Spearman correlation coefficients (R^2) show that insulin secretion data are poorly correlated with SP Ampl. (left), significantly correlated with SP Freq. (middle), and that the combination of both Freq. and Ampl. (see the formula detailed above) fully predicts insulin secretion (N = 4 independent experiments).

Multicellular SPs Drive the Biphasic Electrical Encoding

We next addressed the relationship between single-cell APs and multicellular SPs and their respective contribution to the biphasic encoding. Low signal-to-noise ratio of metal electrodes at high frequencies prevents the analysis of APs (29). Therefore, we switched to PEDOT-MEAs with electroactive polymer-covered electrodes (Fig. 4*A*), which optimized AP detection (29) (Fig. 4*B*). The duration of extracellular APs was ∼100 ms (Fig. 4*C*), as expected (38). Islets were stimulated by glucose within a narrow physiological range (5.5–8.2 mmol/L), different from supraphysiological levels used in our previous studies (29–32). A measurement of 5.5 mmol/L glucose appeared to be the threshold concentration since a small biphasic response was observed for SPs but not for APs, whereas 6 and 8.2 mmol/L glucose triggered strong biphasic activities for both SPs and APs (Fig. 4*D*) in ∼90% of islets (Supplementary Fig. 3*A*) after a short delay (Supplementary Fig. 3*B*). At 5.5 mmol/L glucose, 45% of islets responded (Supplementary Fig. 3*A*) with a longer delay (Supplementary Fig. 3*B*). At this threshold concentration, the presence of SPs, but of small amplitudes and with few APs (Fig. 4*D* and *E*), is in line with intracellular recordings in intact islets (39) and may be explained by some β-cells with some K_{ATP} channel activity at 5.5 mmol/L glucose sufficient to restrain signal propagation.

We also observed further differences in glucose concentration dependency (Fig. 4*E*). SP amplitudes increased during the first and second phase between 5.5 and 6 mmol/L glucose but remained stable upon a further increase in glucose. In contrast, frequencies of SPs and APs continued to augment until 8.2 mmol/L glucose mainly in the second phase. As maximal SP amplitude represents the size of the functional cell clusters, clusters increase significantly between the two phases for all tested concentrations (Supplementary Fig. 3*C*). Collectively, these data suggest that increasing glucose from 3 to 8.2 mmol/L recruits more islets and generate more active cell clusters (SP frequency), whereas maximal cluster size is reached already at 6 mmol/L glucose (SP amplitude).

To understand the relative contribution of multicellular and unicellular signals during the transition between first and second phase, SP and AP kinetics were normalized. SP and AP kinetics were similar for the first phase at 5.5 and 6 mmol/L glucose (Fig. 4*F*, left and middle). Major differences were evident in the second phase at these two concentrations: the small second phase at 5.5 mmol/L glucose involved mainly SPs. Although biphasic patterns of APs started to appear at 6 mmol/L, SPs were still more pronounced especially at the beginning of the second phase as evidenced by differences in the area under the curve (ΔAUC) of the respective signals. Moreover, even at 8.2 mmol/L, SPs were far more prominent than APs during the nadir and beginning of the second phase (Fig. 4*F*, right), a period when insulin secretion persists, albeit at a lower level (Fig. 2). The subsequent development of SPs during the second phase indicates that β-cells synchronize, probably once they are in a metabolic steady state with K_{ATP} channels blocked to a similar extent. Hence, SP dynamics accurately mirror insulin secretion patterns as

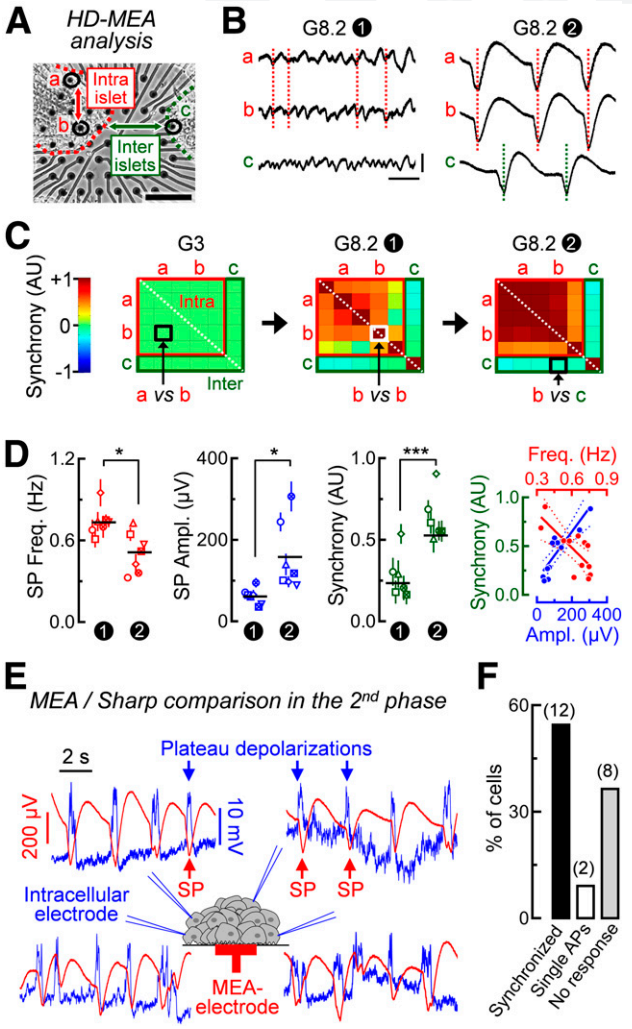

Figure 3—Intraislet coupling increases in the second phase as revealed by HD-MEAs and by simultaneous extracellular and intracellular recordings. *A*: Two mouse islets on an HD-MEA. Circled electrodes contacting the same islet (intraislet) or different islets (interislets) are presented in *B* and *C*. Scale bar: 100 μm. *B*: SPs on the three electrodes presented in *A* during the two phases (❶ and ❷) at G8.2. Red dotted lines indicate synchrony between intraislet electrodes. This intraislet synchrony increases from the first to the second phase. No synchrony was observed between interislet electrodes (green dotted lines). Scale bars: 2 s (horizontal) and 100 μV (vertical). *C*: Representative correlation matrices obtained at different time points (G3; G8.2 first and second phase) comparing the SP synchrony between intra- and interislet electrodes (see Supplementary Methods and Supplementary Fig. 1 for the generation of correlation matrices). The color code is given on the left with arbitrary units (AU): +1, complete synchrony (e.g., when one electrode is compared with itself such as b vs. b); 0, no synchrony or no SPs; and −1, opposition of phases). Correlations between electrodes depicted in *A* and *B* are given as examples. *D*: Seven islets (N = 7, n = 2–13 electrodes each) were analyzed on HD-MEAs. Left three panels: means (± SEM) of frequency (Freq.), amplitude (Ampl.), and intraislet synchrony of SPs for the two phases at G8.2. Each symbol corresponds to one islet. Black horizontal lines indicate means of all islets. *$2P < 0.05$; ***$2P < 0.001$. Right panel: synchrony of SPs is correlated with SP amplitude (Spearman correlation test: $R^2 = 0.77$; ***$2P = 0.0003$; $n = 12$) and inversely correlated with SP frequency ($R^2 = 0.56$; **$2P = 0.0062$; $N = 6$ islets, $n = 12$). *E*: Simultaneous extracellular and intracellular recordings of a mouse islet. Glucose-evoked SPs generated by an islet were recorded extracellularly with an MEA-electrode (red). At the same time, an intracellular sharp microelectrode was introduced into different cells of the same islet. Intracellular plateau depolarizations (blue) were systematically synchronized with SPs. *F*: Proportions of: *1*) cells with plateau depolarizations in synchrony with SPs as in *E*, *2*) cells with continuous single AP patterns instead of plateau depolarizations, and *3*) cells without glucose response. In parentheses are the numbers of cells (recorded on five different MEAs).

compared with APs, confirming that they represent the master electrical signal encoding biphasic secretion.

The Three-Dimensional Structure of Islets and Physiological Levels of Ca^{2+} Are Required for Optimal Connectivity and Biphasic Responses

To ascertain that not only signals from the outer layer of islet cells contribute, we also performed experiments in two-dimensional (2D) monolayers of islet cells (Supplementary Fig. 4). Biphasic behavior was observed in this configuration, but SPs were reduced in the second phase, in line with a 2D coupling in monolayers versus a three-dimensional connectivity in islets (Supplementary Fig. 4*A* and *B*). Furthermore, SPs were of higher amplitudes in large monolayers than in medium and small ones, which confirms that SP amplitudes reflect the size of functional β-cell clusters (Supplementary Fig. 4*C* and *D*). We would also like to stress that our recordings were performed with physiological glucose and extracellular Ca^{2+} concentrations. Indeed, supraphysiological Ca^{2+} levels exceeding twice the normal concentrations are often used (5,18,37), but create artifactual coupling patterns altering SP and AP dynamics (Supplementary Fig. 5).

Physiological Postprandial Levels of GLP-1 Act Only on the Second Phase by Enhancing Multicellular Coupling Signals (SPs) in Mouse and Human Islets

Intestinal incretin hormones such as GLP-1 are major modulators of insulin secretion. Effects of postprandial levels of GLP-1 on the two phases of islets activation have never been assessed. Moreover, GLP-1 has rarely been used at physiological picomolar concentrations (32,40), and different pathways may be activated at pharmacological nanomolar concentrations (40). We therefore stimulated the same mouse islets with different glucose concentrations in the absence or presence of 50 pmol/L GLP-1 during both phases. At 5.5 mmol/L glucose, only very weak responses were observed (Fig. 5*A*) in few islets (Fig. 5*C*, top), but in the presence of GLP-1, a far greater number of islets became glucose responsive (Fig. 5*C*, top), and the hormone considerably amplified the second phase (Fig. 5*A* and *D*). To confirm that the effect is restricted to the second phase, we examined the effect of picomolar GLP-1 at 8.2 mmol/L glucose. Islets generated two electrical phases for SPs and APs (Fig. 5*B*), and GLP-1 did not recruit more active islets at this glucose concentration (Fig. 5*C*, bottom). Again, GLP-1 specifically increased only the second phase and concerned only multicellular coupling

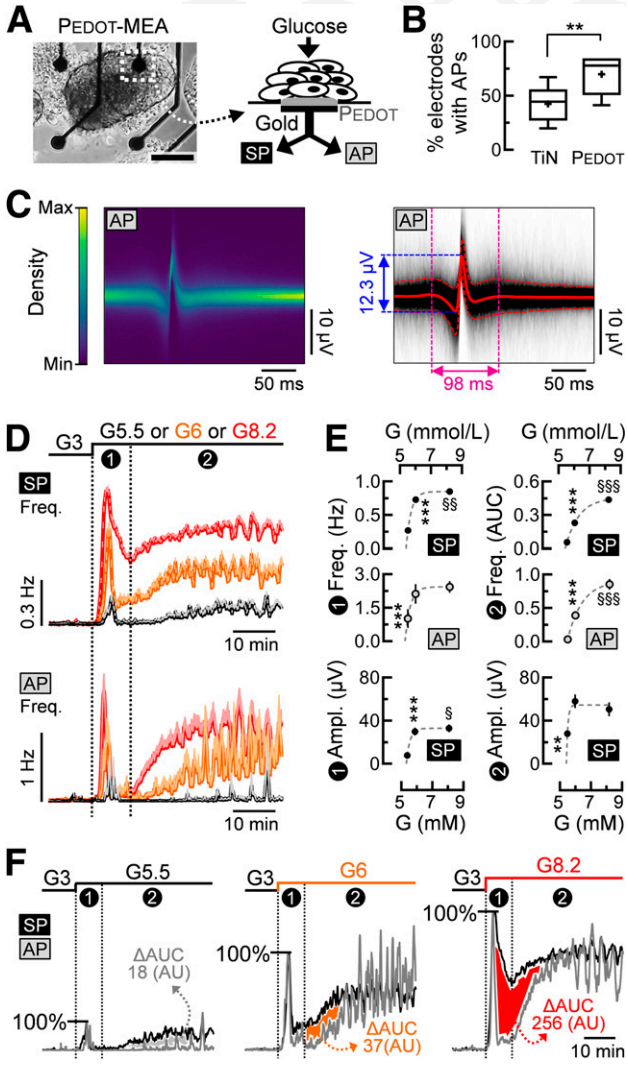

Figure 4—Glucose dependency of multicellular (SP) and unicellular (AP) signal kinetics analyzed with polymer-covered MEA electrodes (PEDOT). *A*: Image (scale bar: 100 µm) and scheme of an islet on a PEDOT-electrode. Metal electrodes are covered with a conductive polymer composed of PEDOT and carbon nanotubes to optimally detect both SPs and APs. *B*: Comparison of metal (TiN) and PEDOT-electrodes regarding the proportion of electrodes with detectable APs (TiN: $N = 21$ MEAs; PEDOT: $N = 7$ MEAs). $^{**}2P < 0.05$. *C*, left: 2D density histogram generated from 21,824 APs ($N = 18$ islets). Sample densities are represented according to the color code in the 2D matrix (time, amplitude). *C*, right: overlay of 21,824 APs (black) and mean ± SD (red) showing extracellular AP duration and amplitude. *D*: Kinetics of SP and AP frequencies (Freq.) (means + SEM) during the two phases evoked by an increase in glucose from G3 to G5.5 (black), G6 (orange), and G8.2 mmol/L (red) ($N = 3$–6, $n = 38$–114). *E*: Statistics. Gray dotted lines: best fitting curves. Top and middle left: peak frequencies of SPs and APs during the first phase (❶) were determined for each electrode. SPs: $^{***}P < 0.001$ for G5.5 vs. G6; §§$P < 0.01$ for G6 vs. G8.2. APs: $^{***}P < 0.001$ for G5.5 vs. G6 and G8.2. Top and middle right: AUCs of SP and AP frequencies during the second phase (❷) normalized over time. $^{***}P < 0.001$ for G5.5 vs. G6; §§§$P < 0.001$ for G6 vs. G8.2. Bottom: maximal amplitudes of SPs (means of the 10th biggest SPs for each electrode) during the two phases. $^{***}P < 0.001$ for G5.5 vs. G6; §$P < 0.05$ for G5.5 vs. G8.2; $^{**}P < 0.01$ for G5.5 vs. G6 and G8.2. See also Supplementary Fig. 3 for complementary analysis. *F*: Comparisons of normalized SP and AP frequency kinetics show that SPs are necessary for the transition between phases. For each glucose concentrations, ΔAUC is given as the difference between normalized AUCs of SP and AP frequencies. AU, arbitrary units.

signal (SPs) without affecting single-cell activities (APs) (Fig. 4*B* and *E*). Note that the activity of islets exhibited oscillations after ~40 min in G8.2 that disappeared upon GLP-1 (Fig. 5*B* and Supplementary Fig. 6), confirming a previous observation that the incretin triggers continuous electrical activity in β-cells (40). Moreover, fitting of SP frequencies showed that picomolar GLP-1 accelerated the appearance of the second phase (Supplementary Fig. 6). Thus, postprandial levels of GLP-1 act only on the second phase by enhancing β-cell cluster activity and coupling. GLP-1 action was also examined in human islets. An increase in glucose provoked SPs with a biphasic profile as in mice, which was less pronounced for APs (Fig. 6*A*). The data confirmed the specific action of GLP-1 in human islets on the second phase of SPs, but not on APs (Fig. 6*B*).

Aging and Glucotoxicity Impair Biphasic Activity

Aging and type 2 diabetes impair not only the overall quantity of insulin secreted, but also the kinetics (10,13,14). The comparison of SP kinetics between young adult and middle-aged mice revealed that both electrical phases were altered by aging (Fig. 7*A*): the reactivity of clusters (SP frequencies) was affected without changes in the extent of coupling (SP amplitudes) (Fig. 7*B*).

Glucotoxicity recapitulates parts of the diabetic state (41). Mouse islets were exposed to a glucotoxic medium (20 mmol/L glucose for 64 h). In these conditions, islets exhibited increased basal SP activities at low glucose (Fig. 7*C* and *D*) in line with the increase in basal secretion in glucotoxicity (41). Upon glucose stimulation, the first phase (i.e., high SP frequencies and low SP amplitudes) was considerably altered (Fig. 7*D*), with a second phase mode starting very early (Fig. 7*C*). Alterations of biphasic activity were confirmed in human islets exposed to glucotoxicity, and these effects were partially reversible, mainly in terms of coupling signals, as indicated by SPs, but not in regard to single-cell activity (APs) (Fig. 8*A* and *B*).

DISCUSSION

Our data provide a new model for the origin of biphasic islet activation based on analysis of single-cell and of micro-organ electrical activity with high spatiotemporal resolution. Our protocols mimicked relevant physiological characteristics in terms of time spans, concentrations of glucose, GLP-1 (42), as well as Ca^{2+} levels, at which the supraphysiological concentrations often used of this cation (5,18,37) considerably distort islet activity.

Our data indicate that progressive multicellular organization establishes the physiological biphasic pattern in both mouse and human islets. Upon glucose stimulation, the first phase originates from a multitude of small β-cell

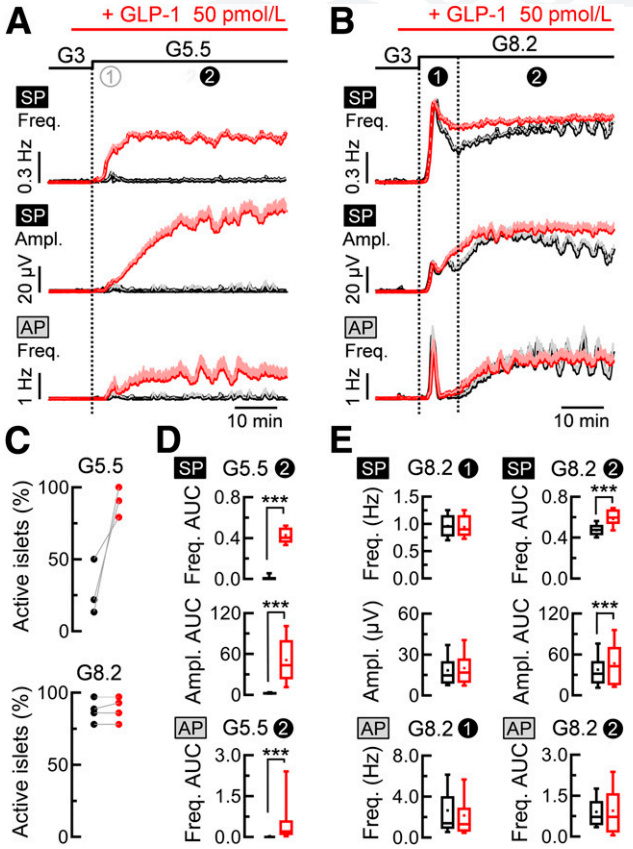

Figure 5—Postprandial levels of GLP-1 act only on the second phase by enhancing multicellular coupling (SP) in mouse islets. *A* and *B*: Mouse islets on PEDOT-MEAs were stimulated by an increase in glucose from G3 to G5.5 (*A*) or to G8.2 (*B*) (black curves). At >100 min later, the same islets were glucose stimulated in the same way but in the presence of 50 pmol/L of GLP-1 applied 5 min before G11 (red curves). Kinetics of SP and AP frequency (Freq.) and SP amplitude (Ampl.) (means + SEM) are given. *C*: Proportion of islets responding electrically to G5.5 or G8.2 with or without GLP-1. *D* and *E*: Statistics on data given in *A* ($N = 3$; $n = 49$ for SPs and $n = 38$ for APs) and *B* ($N = 4$; $n = 64$ for SPs and $n = 41$ for APs). Peak frequency and mean amplitude of SPs and peak frequency of APs during the first phase were determined for each electrode. AUCs of SP frequency, SP amplitude, and AP frequency during the second phase were normalized over time. ***$2P < 0.001$.

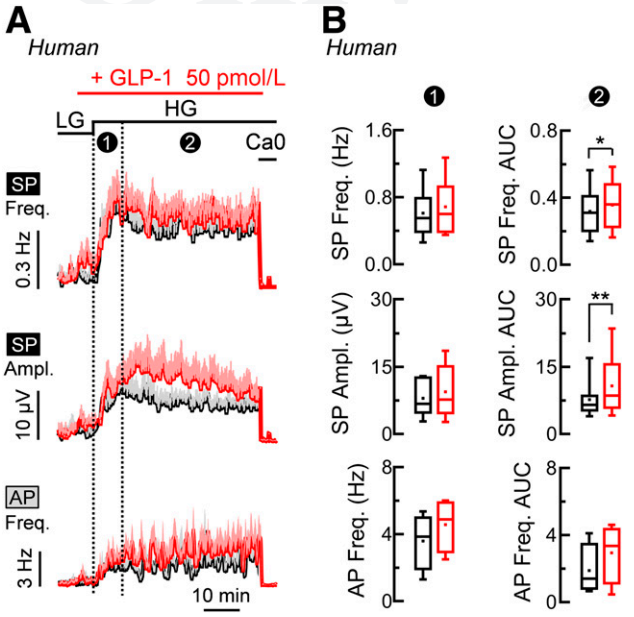

Figure 6—Postprandial levels of GLP-1 act only on the second phase by enhancing multicellular coupling (SP) but not single-cell activities (AP) in human islets. *A*: Human islets on a PEDOT-MEA were stimulated by an increase in glucose from 1 mmol/L (low glucose [LG]) to 11 mmol/L (high glucose [HG]) (black). At >100 min later, the same islets were stimulated in the same way by glucose but in the presence of 50 pmol/L of GLP-1 applied 5 min before HG (red). Note that, under these conditions, two consecutive electrical responses to G11 only were similar. Kinetics of SP frequencies (Freq.) and amplitudes (Ampl.) and of AP frequencies before and during the two phases are given (means + SEM). Note that first phases were less marked for APs than for SPs. At the end of the protocol, a solution depleted in Ca^{2+} (Ca0) was applied to determine the basal activity. *B*: Statistics ($n = 4$–10). ❶: peak frequency of SPs and APs and mean amplitude of SPs during the first phase were determined for each electrode. ❷: AUCs of SP frequency, SP amplitude, and AP frequency during the second phase normalized over time. *$2P < 0.05$; **$2P < 0.01$.

clusters, highly active but poorly coordinated, whereas during the subsequent second phase, clusters enlarge and contain less active but highly synchronized β-cells (Supplementary Fig. 7*A* and *B*), in accordance with previous observations using Ca^{2+} imaging in pancreas slices (27). Parallel monitoring of SPs and insulin secretion shows that the overall activity of β-cell clusters in terms of frequency contributes far more than the extent of coupling (given by the amplitude) to biphasic secretion, while the combination of both frequency and coupling is most closely correlated with the biphasic insulin pattern.

The effects of postprandial levels of GLP-1 on both phases were also investigated in this study for the first time in islets. Physiological levels of incretin promote only the second phase by enhancing multicellular signals but not single-cell activities (Supplementary Fig. 7*A* and *B*). GLP-1 increases the size of clusters (SP amplitude), their level of activity (SP frequency), and the time spent in active periods. Moreover, GLP-1 also accelerates the installation of the second phase. As the second phase coupling mode constitutes an economic mode, it is certainly more favorable for prolonged activity during the digestion. Its further prominence in the presence of GLP-1 may contribute to protective effects of the incretin on β-cells (43) and certainly underlies its specific secretory effects in vivo on the second phase in humans (44,45). In contrast, aging reduces the reactivity, but not the size, of β-cell clusters, similar to glucotoxicity, for which, in addition, an increased basal activity is observed (Supplementary Fig. 7*A* and *C*).

Biphasic hormone secretion has generally been explained by distinct granule pools (19–21). Differential Ca^{2+} sensitivities and kinetics have been observed by intracellular electrophysiology (46), which records, however, only a fraction of the phases. Interestingly, imaging

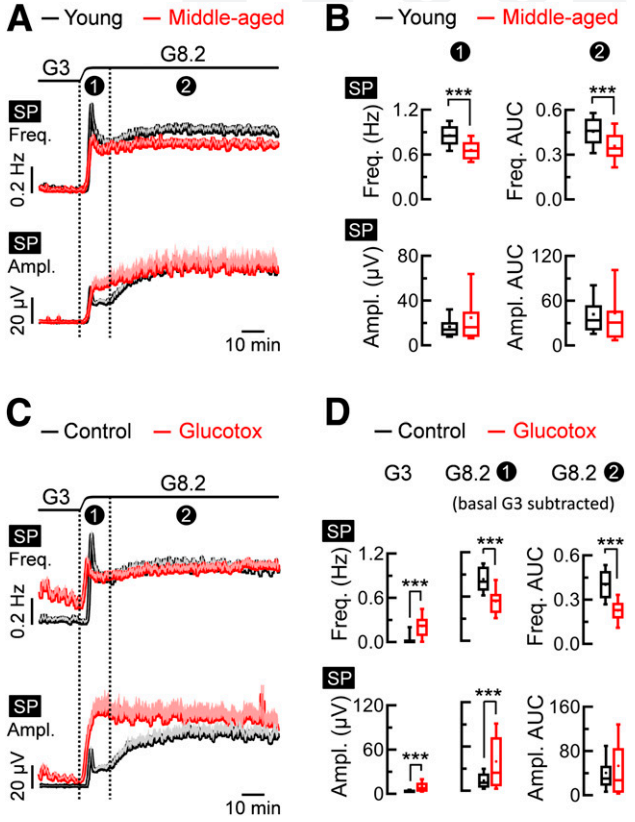

Figure 7—Aging and glucotoxicity alter the biphasic electrical profile of SPs in mouse islets. *A*: Islets from young adult (12–13 weeks, black) or middle-aged mice (39–45 weeks, red) on standard MEAs (metal electrodes) were stimulated by an increase in glucose from G3 to G8.2. Kinetics of SP frequency (Freq.) and amplitude (Ampl.) are given for the two phases (mean + SEM). *B*: Statistics on data in *A* ($N = 3–5$; $n = 46–58$). *B*, left: peak frequency and mean amplitude of SPs during the first phase were determined for each electrode. *B*, right: AUCs of SP frequencies and amplitudes of the second phase normalized over time. ***$2P < 0.001$. *C*: Islets from young adult mice cultured on standard MEAs were stimulated as in *A*, and kinetics of SP frequency and amplitude (means + SEM) were determined as in *A* for the same islets exposed to two conditions: before (culture at 11 mmol/L glucose, Control, black) and 64 h after subsequent culture at 20 mmol/L (Glucotox, red). *D*: Statistics on data in *C* ($N = 3$, $n = 43$). G3: means of SP frequencies and amplitudes over 10 min preceding G8.2. G8.2❶: peak frequencies and mean amplitude of SP during the first phase were determined for each electrode. G8.2❷: AUCs of SP and frequencies and amplitudes of the second phase normalized over time. For G8.2❶ and G8.2❷, basal activities at G3 were subtracted for both control and glucotoxic conditions. ***$2P < 0.001$.

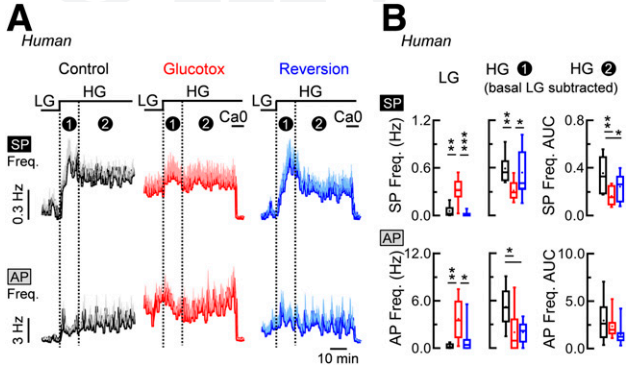

Figure 8—Glucotoxicity in human islets alters basal activity and biphasic electrical profiles. Human islets cultured on PEDOT-MEAs were stimulated by an increase in glucose from 1 mmol/L (low glucose [LG]) to a high concentration triggering a biphasic electrical response (high glucose [HG], 7 or 11 mmol/L, depending on the donor). *A*: Kinetics of SP and AP frequencies (Freq.) (means + SEM) before and during the two phases were determined for the same islets of the same donors in three consecutive conditions: before (culture at 5.6 mmol/L glucose, Control, black), 64 h after subsequent culture at 20 mmol/L (Glucotox, red), and 69 h after further subsequent culture at 5.6 mmol/L (Reversion, blue). *B*: Statistics ($N = 2$, $n = 10–15$). LG: means of SP and AP frequency before HG. HG❶: peak frequencies of SP and AP during the first phase were determined for each electrode. HG❷: AUCs of SP and AP frequencies of the second phase normalized over time. For HG❶ and HG❷, the basal activity at LG was subtracted in the three conditions. *$P < 0.05$; **$P < 0.01$; ***$P < 0.001$.

vesicle movements does not unambiguously provide support for distinct vesicle pools as a base for biphasic hormone release (19,47). In addition, biphasic β-cell activity requires multicellular processes (22,23). Multicellular SPs drive the transition between phases, and their profiles clearly mirror the biphasic and monophasic insulin secretions evoked by glucose and leucine, respectively (34). Since electrical SPs occur upstream of exocytosis, our data support the view that SPs propagating across islet β-cells constitute the master regulator of biphasic organization. The other biphasic mechanisms observed downstream at the cytoskeleton and insulin granule levels (5,19–21) may represent a precise adaptation contributing to the amplification of biphasic secretion kinetics.

This dynamic organization appears well adapted to physiological and metabolic requirements. Indeed, the high but poorly synchronized activity of the first phase (Supplementary Fig. 7*A* and *B*) provides a rapid and prominent homeostatic response but is rather energy consuming and potentially toxic due to the cytosolic accumulation of Ca^{2+}. In the second phase, an increase in coupling concomitant with a reduction of the overall activity prevents such excesses (Supplementary Fig. 7*A* and *B*) and may constitute a more economical long-term activity.

The considerable reduction of the first electrical phase upon aging and glucotoxicity (Supplementary Fig. 7*A* and *B*) is in line with the clinical data (10–14). Westacott et al. (48) reported that aging alters coupling in mouse and human islets, but the impact on each phase was not addressed. In this study, the reduction in SP frequency in the first phase suggests that the basic organizational mode in clusters is not changed per se during this period, but the overall activity of clusters is decreased. Moreover, increase in basal activity blunted the net increment in second-phase activity contributing to the well-known phenomenon of glucose insensitivity (49).

The unbiased long-term approach used in this study provides a new model of islet activation and its derangements. The methodology may be of considerable value to

evaluate disease models and maturation; for example, in the setting of normal or patient-obtained stem cell–derived surrogate islets. Finally, better understanding of islet endogenous algorithms as presented in this study may also improve development of new commands driving insulin pumps for the therapy of diabetes (50).

Acknowledgments. The authors thank the colleagues at the University of Bordeaux Animal Facility for help.

Funding. This study was supported by the following grants: European Regional Development Fund Diaglyc (to J.L. and S.R.), Agency Nationale de la Recherche ANR-18-CE17-0005 DIABLO (to J.L. and S.R.), Ministère de l'Education Nationale, de l'Enseignement Superieur et de la Recherche Excellence PhD Scholarship (to M.R. and M.J.), and Université de Bordeaux PEPS Idex/CNRS (to M.R.).

Q:2 **Duality of Interest.** No potential conflicts of interest relevant to this article were reported.

Author Contributions. M.J., J.L., and M.R. conceived the study. M.J., E.B., A.P., E.P., J.G., S.O., D.C., and M.R. performed experiments. M.J., E.B., A.P., J.L., and M.R. analyzed data. M.J., J.L., and M.R. wrote the manuscript. F.L. and D.B. provided human islets. B.C., S.R., J.L., and M.R. procured funding. M.R. is the guarantor of this work and, as such, had full access to all of the data in the study and takes responsibility for the integrity of the data and the accuracy of the data analysis.

Prior Presentation. Parts of this study were presented as abstracts and oral communications at the annual meeting of the European Association for the Study of Diabetes, Berlin, Germany, 1–5 October, 2018, Congress of the Société Francophone du Diabète, Nantes, France, 20–23 March 2018, and the Keystone Symposia, Islet Biology: From Gene to Cell to Micro-Organ, Santa Fe, NM, 27–31 January 2020.

References

1. Freeman ME, Kanyicska B, Lerant A, Nagy G. Prolactin: structure, function, and regulation of secretion. Physiol Rev 2000;80:1523–1631
2. Kadota C, Ohta M, Takahashi M. Dynamic response to follicle-stimulating hormone of secretion of progesterone by superfused rat ovarian granulosa cells. Mol Cell Endocrinol 1988;59:213–220
3. Voets T, Neher E, Moser T. Mechanisms underlying phasic and sustained secretion in chromaffin cells from mouse adrenal slices. Neuron 1999;23:607–615
4. Grodsky GM. A threshold distribution hypothesis for packet storage of insulin and its mathematical modeling. J Clin Invest 1972;51:2047–2059
5. Rorsman P, Ashcroft FM. Pancreatic β-cell electrical activity and insulin secretion: of mice and men. Physiol Rev 2018;98:117–214
6. Henquin JC, Nenquin M, Stiernet P, Ahren B. In vivo and in vitro glucose-induced biphasic insulin secretion in the mouse: pattern and role of cytoplasmic Ca^{2+} and amplification signals in beta-cells. Diabetes 2006;55:441–451
7. Robbins DC, Jaspan J, Vasquez B, Van Cauter E. Biphasic patterns of peripheral insulin and glucose levels after lunch in normal subjects. Diabetes Care 1987;10:293–299
8. Nunemaker CS, Wasserman DH, McGuinness OP, Sweet IR, Teague JC, Satin LS. Insulin secretion in the conscious mouse is biphasic and pulsatile. Am J Physiol Endocrinol Metab 2006;290:E523–E529
9. Tokarz VL, MacDonald PE, Klip A. The cell biology of systemic insulin function. J Cell Biol 2018;217:2273–2289
10. Del Prato S. Loss of early insulin secretion leads to postprandial hyperglycaemia. Diabetologia 2003;46(Suppl. 1):M2–M8
11. Stumvoll M, Fritsche A, Häring HU. Clinical characterization of insulin secretion as the basis for genetic analyses. Diabetes 2002;51(Suppl. 1):S122–S129
12. Weiss R, Caprio S, Trombetta M, Taksali SE, Tamborlane WV, Bonadonna R. Beta-cell function across the spectrum of glucose tolerance in obese youth. Diabetes 2005;54:1735–1743
13. Szoke E, Shrayyef MZ, Messing S, et al. Effect of aging on glucose homeostasis: accelerated deterioration of beta-cell function in individuals with impaired glucose tolerance. Diabetes Care 2008;31:539–543
14. Chang AM, Halter JB. Aging and insulin secretion. Am J Physiol Endocrinol Metab 2003;284:E7–E12
15. Luciani DS, Misler S, Polonsky KS. Ca^{2+} controls slow NAD(P)H oscillations in glucose-stimulated mouse pancreatic islets. J Physiol 2006;572:379–392
16. Li J, Shuai HY, Gylfe E, Tengholm A. Oscillations of sub-membrane ATP in glucose-stimulated beta cells depend on negative feedback from $Ca^{(2+)}$. Diabetologia 2013;56:1577–1586
17. Taddeo EP, Stiles L, Sereda S, et al. Individual islet respirometry reveals functional diversity within the islet population of mice and human donors. Mol Metab 2018;16:150–159
18. Gilon P, Henquin JC. Influence of membrane potential changes on cytoplasmic Ca2+ concentration in an electrically excitable cell, the insulin-secreting pancreatic B-cell. J Biol Chem 1992;267:20713–20720
19. Seino S, Shibasaki T, Minami K. Dynamics of insulin secretion and the clinical implications for obesity and diabetes. J Clin Invest 2011;121:2118–2125
20. Henquin JC, Ishiyama N, Nenquin M, Ravier MA, Jonas JC. Signals and pools underlying biphasic insulin secretion. Diabetes 2002;51(Suppl. 1):S60–S67
21. Rorsman P, Eliasson L, Renström E, Gromada J, Barg S, Göpel S. The cell physiology of biphasic insulin secretion. News Physiol Sci 2000;15:72–77
22. Chertow BS, Baranetsky NG, Sivitz WI, Meda P, Webb MD, Shih JC. Cellular mechanisms of insulin release. Effects of retinoids on rat islet cell-to-cell adhesion, reaggregation, and insulin release. Diabetes 1983;32:568–574
23. Head WS, Orseth ML, Nunemaker CS, Satin LS, Piston DW, Benninger RK. Connexin-36 gap junctions regulate in vivo first- and second-phase insulin secretion dynamics and glucose tolerance in the conscious mouse. Diabetes 2012;61:1700–1707
24. Johnston NR, Mitchell RK, Haythorne E, et al. Beta cell hubs dictate pancreatic islet responses to glucose. Cell Metab 2016;24:389–401
25. Salem V, Silva LD, Suba K, et al. Leader β-cells coordinate Ca^{2+} dynamics across pancreatic islets in vivo. Nat Metab 2019;1:615–629
26. Dorrell C, Schug J, Canaday PS, et al. Human islets contain four distinct subtypes of β cells. Nat Commun 2016;7:11756
27. Markovič R, Stožer A, Gosak M, Dolenšek J, Marhl M, Rupnik MS. Progressive glucose stimulation of islet beta cells reveals a transition from segregated to integrated modular functional connectivity patterns. Sci Rep 2015;5:7845
28. Satin LS, Zhang Q, Rorsman P. "Take me to your leader": an electrophysiological appraisal of the role of hub cells in pancreatic islets. Diabetes 2020;69:830–836
29. Koutsouras DA, Perrier R, Villarroel Marquez A, et al. Simultaneous monitoring of single cell and of micro-organ activity by PEDOT:PSS covered multielectrode arrays. Mater Sci Eng C 2017;81:84–89
30. Perrier R, Pirog A, Jaffredo M, et al. Bioelectronic organ-based sensor for microfluidic real-time analysis of the demand in insulin. Biosens Bioelectron 2018;117:253–259
31. Raoux M, Bornat Y, Quotb A, Catargi B, Renaud S, Lang J. Non-invasive long-term and real-time analysis of endocrine cells on micro-electrode arrays. J Physiol 2012;590:1085–1091
32. Lebreton F, Pirog A, Belouah I, et al. Slow potentials encode intercellular coupling and insulin demand in pancreatic beta cells. Diabetologia 2015;58:1291–1299
33. Schreiber S, Fellous JM, Whitmer D, Tiesinga P, Sejnowski TJ. A new correlation-based measure of spike timing reliability. Neurocomputing 2003;52-54:925–931
34. Liu YJ, Cheng H, Drought H, MacDonald MJ, Sharp GW, Straub SG. Activation of the K_{ATP} channel-independent signaling pathway by the nonhydrolyzable analog of leucine, BCH. Am J Physiol Endocrinol Metab 2003;285:E380–E389
35. Buzsáki G, Anastassiou CA, Koch C. The origin of extracellular fields and currents–EEG, ECoG, LFP and spikes. Nat Rev Neurosci 2012;13:407–420

36. Pørksen N, Hollingdal M, Juhl C, Butler P, Veldhuis JD, Schmitz O. Pulsatile insulin secretion: detection, regulation, and role in diabetes. Diabetes 2002; 51(Suppl. 1):S245–S254

37. Zhang M, Goforth P, Bertram R, Sherman A, Satin L. The Ca^{2+} dynamics of isolated mouse beta-cells and islets: implications for mathematical models. Biophys J 2003;84:2852–2870

38. Jacobson DA, Kuznetsov A, Lopez JP, Kash S, Ammälä CE, Philipson LH. Kv2.1 ablation alters glucose-induced islet electrical activity, enhancing insulin secretion. Cell Metab 2007;6:229–235

39. Drews G, Krippeit-Drews P, Düfer M. Electrophysiology of islet cells. Adv Exp Med Biol 2010;654:115–163

40. Shigeto M, Ramracheya R, Tarasov AI, et al. GLP-1 stimulates insulin secretion by PKC-dependent TRPM4 and TRPM5 activation. J Clin Invest 2015;125: 4714–4728

41. Jonas JC, Bensellam M, Duprez J, Elouil H, Guiot Y, Pascal SM. Glucose regulation of islet stress responses and beta-cell failure in type 2 diabetes. Diabetes Obes Metab 2009;11(Suppl. 4):65–81

42. Elliott RM, Morgan LM, Tredger JA, Deacon S, Wright J, Marks V. Glucagon-like peptide-1 (7-36)amide and glucose-dependent insulinotropic polypeptide secretion in response to nutrient ingestion in man: acute post-prandial and 24-h secretion patterns. J Endocrinol 1993;138:159–166

43. Aaboe K, Krarup T, Madsbad S, Holst JJ. GLP-1: physiological effects and potential therapeutic applications. Diabetes Obes Metab 2008;10:994–1003

44. Quddusi S, Vahl TP, Hanson K, Prigeon RL, D'Alessio DA. Differential effects of acute and extended infusions of glucagon-like peptide-1 on first- and second-phase insulin secretion in diabetic and nondiabetic humans. Diabetes Care 2003; 26:791–798

45. Woerle HJ, Carneiro L, Derani A, Göke B, Schirra J. The role of endogenous incretin secretion as amplifier of glucose-stimulated insulin secretion in healthy subjects and patients with type 2 diabetes. Diabetes 2012;61:2349–2358

46. Misler S, Zhou Z, Dickey AS, Silva AM, Pressel DM, Barnett DW. Electrical activity and exocytotic correlates of biphasic insulin secretion from beta-cells of canine islets of Langerhans: contribution of tuning two modes of Ca^{2+} entry-dependent exocytosis to two modes of glucose-induced electrical activity. Channels (Austin) 2009;3:181–193

47. Gandasi NR, Yin P, Omar-Hmeadi M, Ottosson Laakso E, Vikman P, Barg S. Glucose-dependent granule docking limits insulin secretion and is decreased in human type 2 diabetes. Cell Metab 2018;27:470–478.e4

48. Westacott MJ, Farnsworth NL, St Clair JR, et al. Age-dependent decline in the coordinated $[Ca^{2+}]$ and insulin secretory dynamics in human pancreatic islets. Diabetes 2017;66:2436–2445

49. Ferrannini E. The stunned beta cell: a brief history. Cell Metab 2010;11:349–352

50. Steil GM, Grodsky GM. The artificial pancreas: is it important to understand how the β cell controls blood glucose? J Diabetes Sci Technol 2013;7:1359–1369

SUPPLEMENTARY METHODS

The MATLAB script used for intra-islet synchrony analysis (related to **Fig. 3A-D** and **Supplementary Fig. 1**) is detailed bellow.

- evt_correlation.m ----------

```
function [correlation_matrix,gauss_sig] =
evt_correlation(timestamps_in,Fs,sigma_s,varargin)
% evt_correlation.m
% - Computes time correlation between events across N channels. Yields an NxN
correlation matrix and a representation of all events and their region of influence.
%
% Outputs
% - correlation_matrix : Correlation matrix (shows correlation index for channels
(i,j))
% - gauss_sig          : Smooth event signal for every channel
%
% Inputs
% - timestamps_in      : Input timestamps. Cell of vectors (one vector of timestamps
per channel). No unit (Nbr of samples).
% - Fs                 : Sampling frequency (Hz)
% - sigma_s            : width of the gaussian (temporal tolerance for event
correlation)
% - varargin           : additional arguments ('nv' makes the function non-verbose)

% Parse additional arguments
if ~isempty(varargin)
    for i=1:length(varargin)
        if isequal(varargin{i},'nv')
                    % Non-verbose flag
            VERBOSE = 0;
        end
    end
end


% Verbose flag check
if ~exist('VERBOSE')
    VERBOSE = 1;
end


% Check all signals for largest timestamp and preallocate memory for event signals
Nsignals = length(timestamps_in);
Lmax = 0;
for i=1:Nsignals
    sp_timestamps = timestamps_in{i};
    sp_timestamps = sort(sp_timestamps(:));
    tmpmax = max(sp_timestamps);
    if ~isempty(tmpmax)
        Lmax = max(Lmax,tmpmax);
```

```
    end
end

events = zeros(Nsignals,Lmax);


% Generate gaussian waveform
gauss_width_s = 5*sigma_s;
x = -gauss_width_s:1/Fs:gauss_width_s;
sigma = sigma_s;
H = gaussmf(x,[sigma 0]);


% Generate smooth events (convolve event signal with gaussian)
gauss_sig = zeros(Nsignals,Lmax-1); % Preallocate
for i=1:Nsignals
      % Generate event signal
    sp_timestamps = timestamps_in{i};
    sp_timestamps = sort(sp_timestamps(:));
    events(i,sp_timestamps) = 1;
      % Smooth it out
    gauss_sig(i,:) = fastconv(events(i,:),H,0); % Fast convolution (fft, product,
ifft)
end


% Generate correlation matrix
correlation_matrix = zeros(Nsignals,Nsignals);
if ~isempty(gauss_sig)
    k = 0; % Counter to keep track of how many correlations have been computed
    for i=1:Nsignals
        for j=1:Nsignals
            correlation_matrix(i,j) = corr(gauss_sig(i,:)',gauss_sig(j,:)'); % Compute
correlation index for channel couple (i,j)
            k = k+1;
            if VERBOSE % Print progress every 100 correlations computed
                if mod(k,100) == 0
                    disp(['Event correlation: ' num2str(k) ' out of '
num2str(Nsignals*Nsignals) ' done.'])
                end
            end
        end
    end
    if VERBOSE % Success message
        disp(['Event correlation: all done.'])
    end
    correlation_matrix(isnan(correlation_matrix))=0; % Nullify NaN (Not A Number)
values
end

end

- fastconv.m ------------------------------------------------------------------
---
function [y]=fastconv(x, h, dim)

Ly=length(x)+length(h)-1;
Ly2=pow2(nextpow2(Ly));

X=fft(x, Ly2); % Fast Fourier transform
H=fft(h, Ly2); % Fast Fourier transform
```

```
if size(X) ~= size(H)
    H=H';
end
Y=X.*H; % Multiply ffts
y=real(ifft(Y, Ly2)); % Inverse fast Fourier transform

if dim==0 % Yield only center part (preserve signal length, time-aligned)
    y=y(round(length(h)/2):1:Ly-round(length(h)/2));
elseif dim==1 % Real time (preserve signal length, delayed)
    y=y(1:1:length(x));
elseif dim==2 % Full size
    y=y(1:1:Ly);
end
```

SUPPLEMENTARY FIGURES & LEGENDS

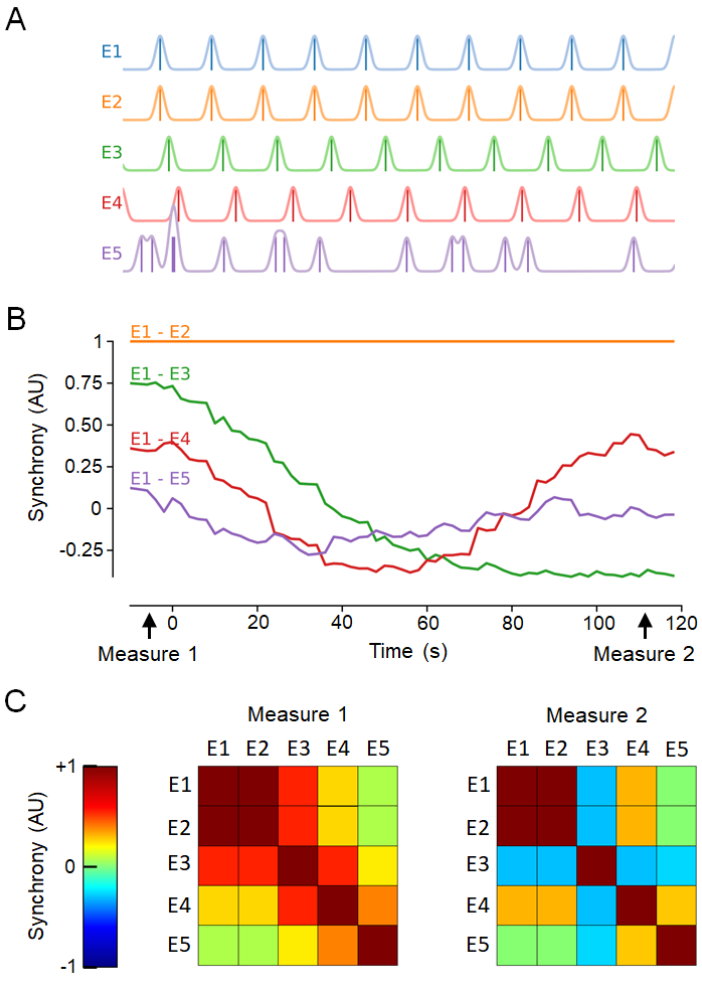

Supplementary Fig. 1. Simulations in MATLAB illustrating the method used to compute temporal event correlations and their matrix representation. To quantify the degree of SP synchrony between electrodes during the biphasic activation, a dynamic code was developed, inspired from works in neurons by Schreiber and colleagues (33). (**A**) Temporal detection of events (vertical lines) and continuous signals constructed by correlating events with Gaussian curves on 5 electrodes (E1 to E5). The time axis is as in (**B**). E1 and E2 are identical trains of regular events. E3 is a regular train of events, at 95% of the speed of E1. E4 is a regular train of events, at 90% of the speed of E1. E5 is a random train of events. (**B**) Time-dependent correlation measurements (synchrony; AU, arbitrary units) between E1 and E2-E5. Colors indicate with which electrode E1 is compared, following the color indicated in (**A**). (**C**) Matrix representations of correlation at the two time points indicated in (**B**). Each square represents the degree of synchrony (color code on the left), between -1 and 1, of the couple of electrodes given by its coordinates (hence the unitary diagonal). The degree of synchrony varies between -1 and +1: +1 representing SPs perfectly synchronized, 0 representing the absence of SP or SPs without any synchrony, and -1 representing SPs in opposition of phases.

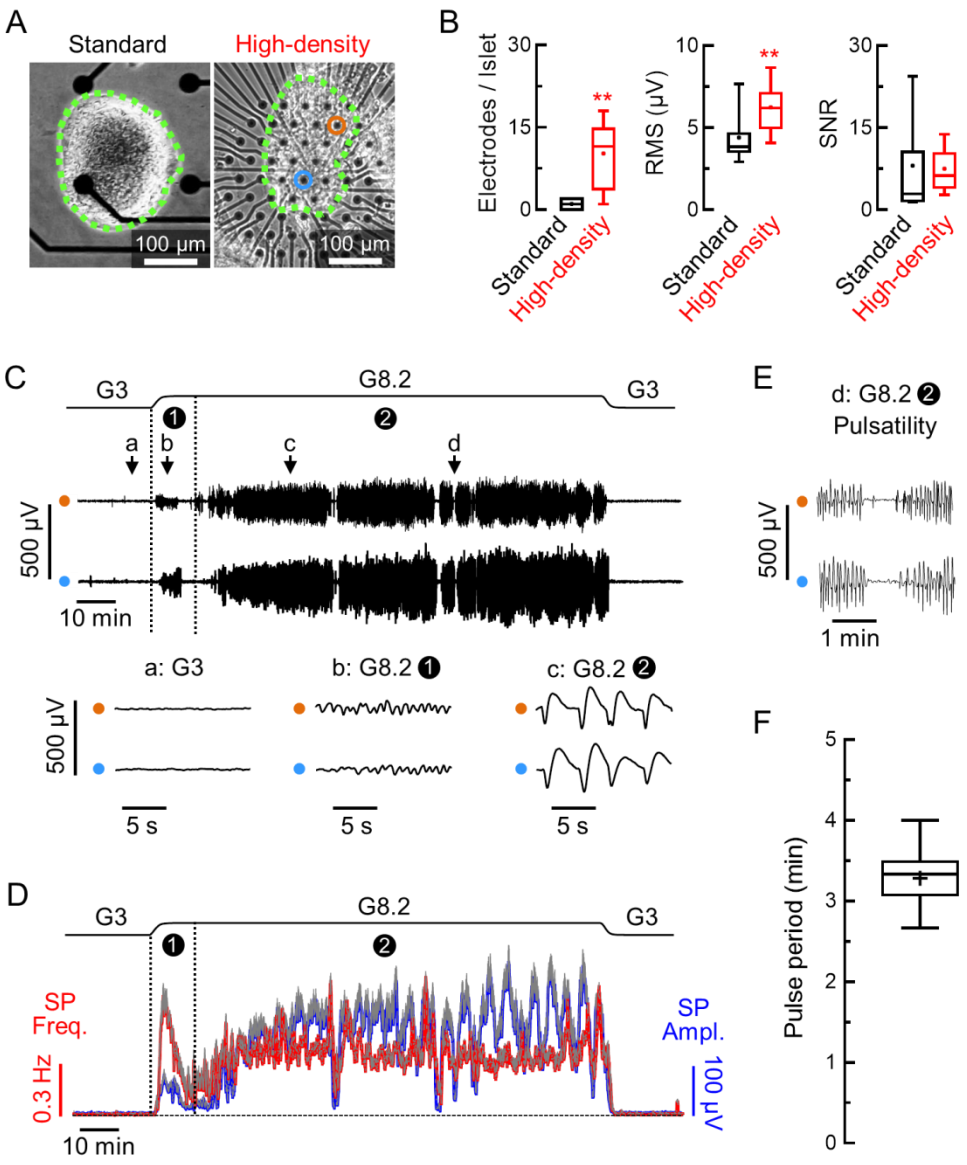

Supplementary Fig. 2. Monitoring of SPs in different regions of an islet with high-density (HD) MEAs. (**A**) Comparison of a standard MEA (4/59 electrodes shown) and a HD-MEA (59/59 electrodes shown). An islet is delimited by green dots. Note the difference between the size of the electrodes (images at identical scales): ø 30 µm for standard MEAs and 10 µm for HD-MEAs. Data from encircled electrodes (orange and light blue) are shown as examples in (**C**) and (**E**) (**B**) HD-MEAs increased the number of electrodes per islets (left panel; N=3-4 MEAs, n=8-49 islets). The smaller electrode diameter increased the noise level (middle panel; root mean square - RMS - noise level, N=3 MEAs, n=12 uncovered electrodes) without affecting the signal-to-noise ratio (SNR) of the very robust SPs (right panel, N=3 MEAs, n=26-30). The RMS noise level was measured with Spike2 on unfiltered traces with a time constant of 5 s and the SNR was taken as the ratio of RMS noise levels between covered and uncovered electrodes when islets were stimulated by glucose ≥8.2 mM for >20 min. ** 2p<0.01, *** 2p<0.001. (**C**)

Top traces: representative recordings of SPs from the 2 electrodes indicated in orange and light blue in (**A**) during the 1st (❶) and the 2nd (❷) phases induced by G8.2 and during the decrease of glucose level to G3. See methods for the optical determination of the kinetics of changes in glucose concentrations (black line at the top). Bottom traces: portions of top traces with higher temporal resolution at the timestamps indicated by a, b and c. (**D**) Kinetics of SP frequency (red) and amplitude (blue) measured in a mouse islet on a HD-MEA (means +SEM, n=13 electrodes) during the 1st (❶) and the 2nd (❷) phases induced by G8.2 and during the decrease of glucose level to G3. (**E**) Portions of top traces shown in (**C**) with higher temporal resolution at the timestamp d showing the appearance of SP pulsatility during the 2nd phase. (**D**) Period of the pulsatility (number of pulses per min) measured after 40 min at G8.2 and during 40 min (N=7 islets).

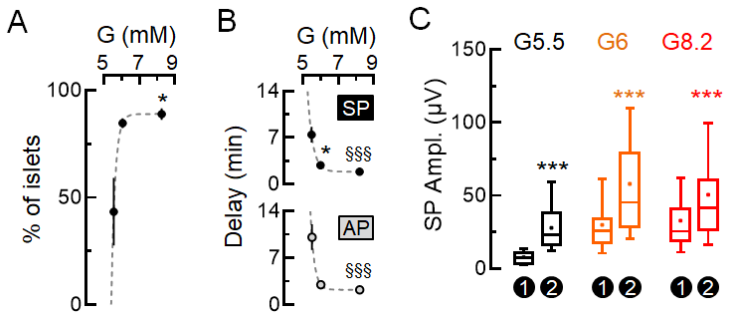

Supplementary Fig. 3. SP and AP analysis in response to glucose. Concentration-dependencies to glucose (G) of the electrical responses generated by mouse islets were analyzed with polymer-coated MEA-electrodes. (**A**) Proportion of islets (means ±SEM) responding electrically to G5.5, G6 and G8.2. * $p<0.01$ for G8.2 vs. G5.5. (**B**) Delays (means ±SEM) between the change in concentration and the first SPs (top) and APs (bottom). * $p<0.05$ for G5.5 vs. G6 and §§§ $p<0.001$ for G8.2 vs. G5.5 and G6. Gray dotted lines are the best fitting curves. (**C**) Statistics comparing maximal amplitude of SPs (means of the 10th biggest SPs for each electrode) during the 1st (❶) vs. the 2nd (❷) phase for each glucose concentration. *** $2p<0.001$. (N=3-6, n=29-114).

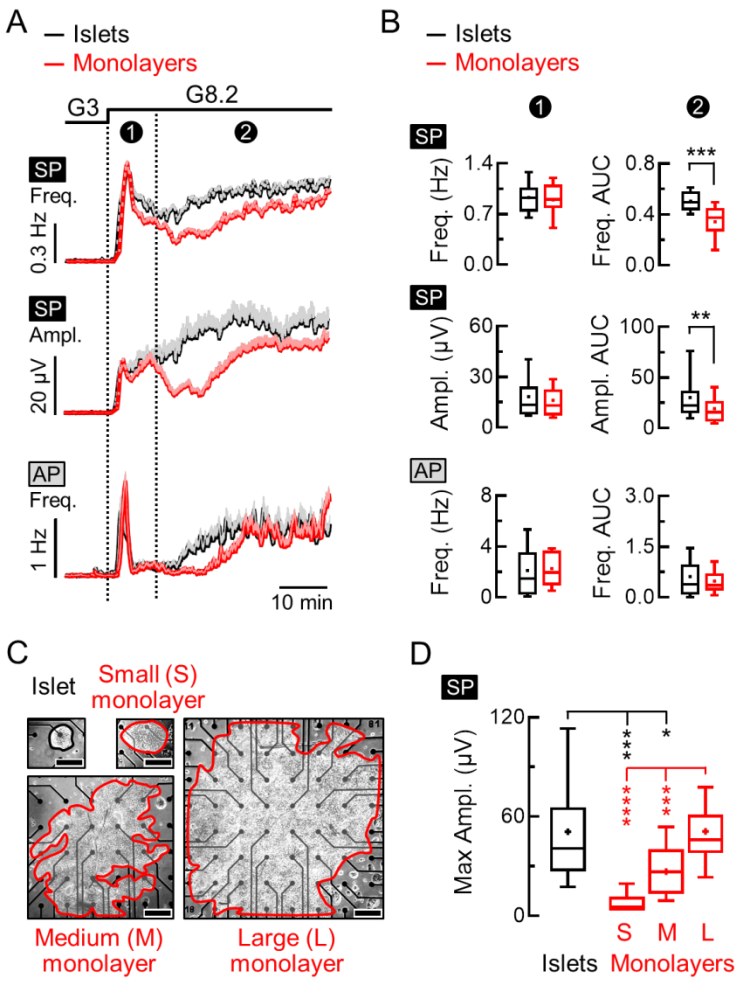

Supplementary Fig. 4. SP and AP analysis of islets versus islet cell monolayers on polymer-coated MEA-electrodes. (**A** and **B**) Comparison of glucose-induced electrical responses of native islets and islet cell monolayers. (**A**) Mouse entire islets (black) or mouse islet cells in monolayers (red) cultured on PEDOT-MEAs were stimulated by an increase in glucose from G3 to G8.2. Kinetics of SP frequency and amplitude as well as AP frequency during the two phases were evaluated (means +SEM). (**B**) Statistics on data in (**A**) (N=3, n=40-80). Left: peak frequency and mean amplitude of SPs and peak frequency of APs during the 1st phase were determined for each electrode. Right: AUCs of SP frequency, SP amplitude and AP frequency during the 2nd phase normalized over time. (**C**) Influence of the size of islet cell monolayers on the maximal amplitude of SPs. Left: representative images (scale bars 200 µm) of an islet (surrounded in black) and a small (<0.1 mm^2), a medium (0.1-0.5 mm^2) and a large (>0.5 mm^2) islet-cell monolayer (surrounded in red). Right: maximal amplitudes of SPs (means of the 10th biggest SPs during the 2nd phase) of islets, small (S), medium (M) and large (L) islet-cell monolayers (n=6-46). * 2p<0.05, ** 2p<0.01, *** 2p<0.001, **** 2p<0.0001.

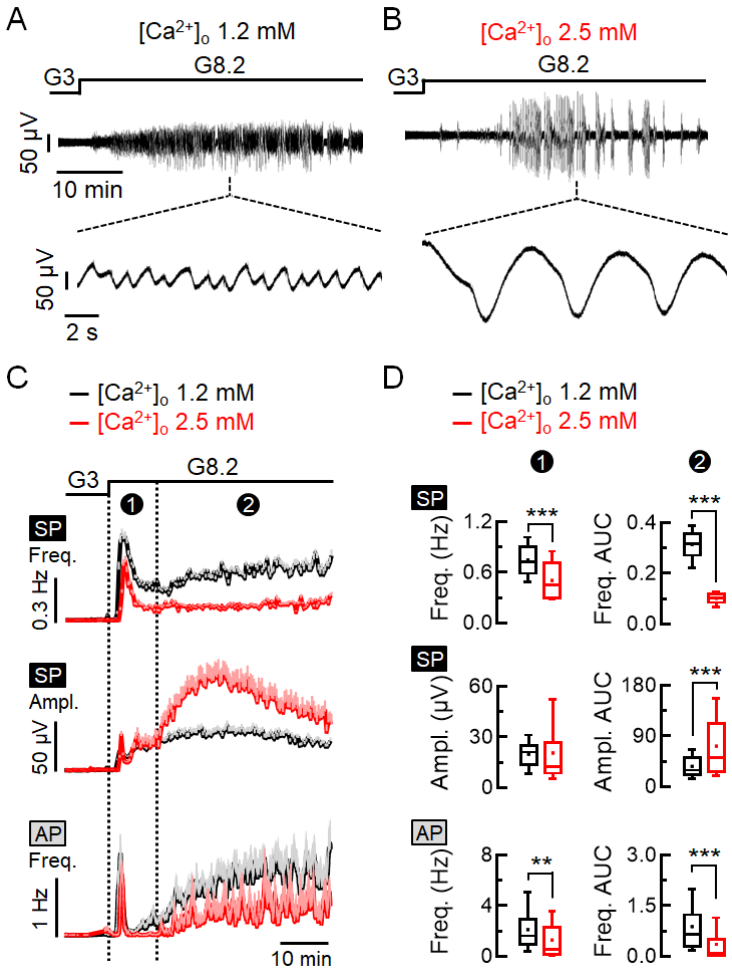

Supplementary Fig. 5. Supraphysiological extracellular Ca^{2+} levels considerably alter SP and AP dynamics. (**A** and **B**) Top traces: representative recordings of the electrical activity of the same mouse islet stimulated by an increase in glucose from G3 to G8.2 in the presence of two different concentrations of extracellular Ca^{2+} ($[Ca^{2+}]_o$) as indicated (PEDOT-MEA; Bandpass: 0.1-700 Hz). Bottom traces: portions of top traces at higher temporal resolution (representative of n=26 recordings from N=3 independent biological preparations). (**C**) Kinetics of SP frequency and amplitude as well as AP frequency during the two phases in the two Ca^{2+} conditions (means +SEM). Similar results were obtained regardless of the concentration of Ca^{2+} tested first (N=3). (**D**) Statistics (N=3; n=26 for SPs and n=20 for APs). Left: peak frequency and mean amplitude of SPs and peak frequency of APs during the 1st phase were determined for each electrode. Right: AUCs of SP frequency, SP amplitude and AP frequency during the 2nd phase normalized over time. ** 2p<0.01, *** 2p<0.001.

A

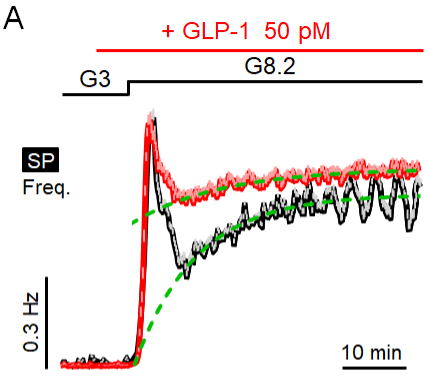

B

One-phase decay	Ctr	GLP-1
Y0 (s)	-544.52	-6
Plateau (Hz)	0.468	0.6202
K	0.002291	0.001191
Half Life (s)	302.5	582.1
Tau (s)	436.4	839.8

Supplementary Fig. 6. Physiological (picomolar) levels of GLP-1 increase and promote the passage from the 1st to the 2nd phase. (**A**) SP frequency kinetics and best fits (green) of the 2nd phase obtained on mouse islets stimulated by increasing glucose from G3 to G8.2 in the absence (black) and in the presence of GLP-1. GLP-1 was applied 5 min before changing glucose concentrations and was present during the stimulation by G8.2 (means +SEM; N=4-6, n=64). (**B**) Details of the fitting curve parameters for the stimulation with G8.2 alone (Ctr) and with G8.2 and GLP-1.

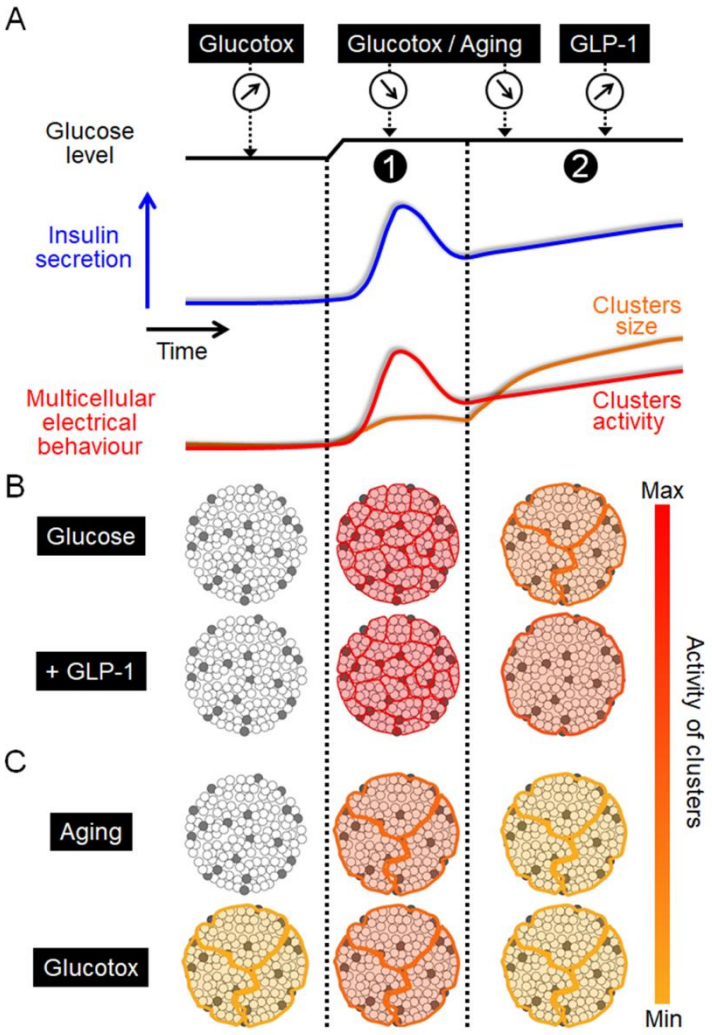

Supplementary Fig. 7. Proposed functional model. (**A**) Biphasic insulin secretion induced by glucose and corresponding multicellular electrical behavior of islets in terms of activity (i.e. SP frequency) and of cluster sizes (i.e. SP amplitude). Modulations of phases in physiological and pathophysiological conditions are indicated on top. (**B** and **C**) Representation of the multicellular behavior of an islet during glucose-induced phases in different physiological and pathophysiological conditions. Unfilled and filled circles represent β and non-β-cells, respectively. Intra-islet clusters are represented by colored areas. Relative sizes of clusters are represented, as well as their level of activity with the color code on the right. (**B**) Model in physiological conditions: upon glucose stimulation, the 1st phase originates from a multitude of highly active small β-cell clusters, but poorly coordinated together, whereas during the subsequent 2nd phase, clusters enlarge and contain less active but highly synchronized β-cell clusters. Physiological levels of GLP-1 promote only the 2nd phase by enhancing multicellular signals (size and activity of clusters). (**C**) Model in aging and glucotoxicity (glucotox). Aging reduces the reactivity, but not the size, of β-cell clusters, similarly to glucotoxicity for which in addition an increased basal activity is observed.